

Lawrence Berkeley National Laboratory

Lawrence Berkeley National Laboratory

Title

Analysis of pumping-induced unsaturated regions beneath a perennial river

Permalink

<https://escholarship.org/uc/item/16k7h98d>

Authors

Su, G.W.
Jasperse, J.
Seymour, D.
et al.

Publication Date

2008-06-24

Peer reviewed

Analysis of Pumping-Induced Unsaturated Regions Beneath a Perennial River

Grace W. Su^{1,*}, James Jasperse², Donald Seymour², James Constantz³, and Quanlin Zhou¹

¹Lawrence Berkeley National Laboratory, Earth Sciences Division, Berkeley, CA, 94720

²Sonoma County Water Agency, Santa Rosa, CA, 95403

³U.S. Geological Survey, Menlo Park, CA, 94025

*corresponding author, now at CalStar Cement, 6851 Mowry Ave, Newark, CA 94560
phone: 510-793-9500; email: graces@calstarcement.com

Preprint of manuscript accepted into *Water Resources Research*

May 2007

ABSTRACT

The presence of an unsaturated region beneath a streambed during groundwater pumping near streams reduces the pumping capacity when it reaches the well screens, changes flow paths, and alters the types of biological transformations in the streambed sediments. A three-dimensional, multi-phase flow model of two horizontal collector wells along the Russian River near Forestville, California was developed to investigate the impact of varying the ratio of the aquifer to streambed permeability on (1) the formation of an unsaturated region beneath the stream, (2) the pumping capacity, (3) stream-water fluxes through the streambed, and (4) stream-water travel times to the collector wells. The aquifer to streambed permeability ratio at which the unsaturated region was initially observed ranged from 10 to 100. The size of the unsaturated region beneath the streambed increased as the aquifer to streambed permeability ratio increased. The simulations also indicated that for a particular aquifer permeability, decreasing the streambed permeability by only a factor of 2 - 3 from the permeability where desaturation initially occurred resulted in reducing the pumping capacity. In some cases, the stream-water fluxes increased as the streambed permeability decreased. However, the stream water residence times increased and the fraction of stream water that reached the wells decreased as the streambed permeability decreased, indicating that a higher streambed flux does not necessarily correlate to greater recharge of stream water around the wells.

1. INTRODUCTION

Water supply and quality have become increasingly important issues for water resources management because of greater water demand and degradation of water quality. As surface water supplies become more contaminated, groundwater near streams is increasingly being utilized as a higher quality source of water. An understanding of stream-groundwater interactions is essential for management of water resources in regions where near-stream groundwater pumping occurs. Recent investigations have demonstrated that using heat as a tracer is an effective tool for quantifying stream-groundwater exchanges (e.g., Anderson, 2005; Stonestrom and Constantz, 2003). Temporal changes in stable isotope measurements, chloride concentrations, and specific conductance have also been used to estimate travel times from the river to nearby wells (e.g., Schubert, 2002; Sheets et al., 2002; Constantz et al., 2003; Hunt et al., 2005; Cox et al., 2007). Time-series data collection combined with simulation of stream-groundwater exchanges yield continuous estimates of streambed permeability parameters, such as the spatial and temporal variability in saturated and unsaturated conductivities. Furthermore, simulation modeling aids in identifying optimal locations for collector wells and monitoring equipment by focusing on critical regions. Thus, development of an appropriate simulation model should be performed in tandem with, or even precede, time-series data campaigns.

In areas where near-stream groundwater pumping occurs, an unsaturated region sometimes develops beneath the streambed. The presence of an unsaturated region can result in production capacity reduction, changes in flow paths, and alteration of the chemical and biological transformations (Greskowiak et al., 2005) compared to what occurs when the region below the

streambed is saturated. An analytical solution for drawdown during groundwater pumping next to a stream with a low permeability streambed layer was derived by Hunt (1999), but this formulation did not consider the formation of an unsaturated region beneath the river. Fox and Durnford (2003) derived an analytical expression for the extent of an unsaturated region beneath a river when a single conventional vertical well pumped adjacent to a stream. Bakker et al. (2005) developed a multilayer approach for modeling groundwater flow to radial collector wells which included the skin effects and internal friction losses. Their study examined flow near collector wells in an unconfined aquifer under saturated conditions, but they did not consider groundwater pumping from the collector wells near a stream.

During losing flow conditions, a hydraulically disconnected region can form beneath a surface water body even without groundwater pumping depending on the permeability contrast between the bed of the water body (i.e., lake bed, streambed) and the aquifer below. Lake beds and streambeds tend to accumulate fine materials during losing conditions, which can establish a permeability contrast and a subsequent unsaturated zone beneath the bed material. Peterson and Wilson (1987) simulated steady-state flux rates for stream-aquifer systems that were hydraulically connected and disconnected, and Rosenberry (2000) observed an unsaturated zone wedge beneath a natural lake and used a two-dimensional variably-saturated flow model to simulate the development of this unsaturated region. During recharge below ephemeral streams, hydraulically connected and disconnected streams have been also observed and modeled (e.g., Wilson and DeCook, 1968; Reid and Dreiss, 1990).

The Sonoma County Water Agency (SCWA) operates six horizontal collector wells adjacent to the Russian River near Forestville, California with a maximum production capacity of over 14,500 m³/hr (92 million gallons per day) in addition to 3200 m³/hr (20 mgd) of standby capacity. These facilities utilize natural filtration processes to provide water supply for over 500,000 people in Sonoma and Marin Counties. Field observations at the SCWA facilities (Figure 1) indicate that an unsaturated region exists beneath the streambed during certain periods of the year near two adjacent horizontal collector wells located along the riverbank. The analytical expression derived by Fox and Durnford (2003) for determining the extent of the unsaturated region for a vertical well is not applicable at the Russian River site because the collector wells consist of nine pipes that extend horizontally and radially. Understanding the conditions that give rise to the unsaturated region beneath the streambed near these horizontal collector wells is critical for gaining a better understanding of surface-groundwater interactions, and the planning, design, and operation of near-stream groundwater pumping facilities.

At the SCWA facilities, an inflatable dam is raised over the spring to fall months to enhance water production capacity, creating a backwater that produces lower velocities and higher temperatures in the river. This results in the deposition of fine-grained sediment and increased organic matter plugging the streambed, which can reduce the streambed permeability (Su et al., 2004; Gorman, 2004). Streambed permeability is a key parameter controlling the development of an unsaturated region beneath the streambed because it controls the flux of river water entering and recharging the aquifer. To investigate the conditions when an unsaturated region forms beneath the streambed during near-stream groundwater pumping, a three-dimensional, multi-phase flow and transport model was developed for the region around the two collector wells at

the Russian River Bank Filtration Facility (Figure 1). In this study, we focus on examining the impact of varying the ratio of the aquifer to streambed permeability on (1) the formation of an unsaturated region beneath the stream, (2) the pumping capacity, (3) stream-water fluxes through the streambed, and (4) stream-water travel times to the collector wells.

2. SIMULATION SETUP

A three-dimensional numerical model was constructed for the region near two collector wells denoted as Collector Wells 1 and 2 using TOUGH2 (Pruess et al, 1999), a multi-phase, subsurface flow and transport model. This reach of the Russian River is underlain by alluvium and river channel deposits, which consist of unconsolidated sands and gravels, interbedded with thin layers of silt and clay. For the area pertaining to this study, the alluvial aquifer is bounded by metamorphic bedrock (e.g., Franciscan Formation) and is considered impermeable relative to the alluvial materials (California Department of Water Resources, 1983). Immediately downstream of this reach bedrock outcrops restrict flow, resulting in naturally increased stream stage and groundwater levels, creating a preferred environment for groundwater extraction.

Oriented along a north-south section of the river, the collector wells reside on the east bank (left bank by protocol) and consist of nine perforated pipes that are projected horizontally from a central caisson into the aquifer at a depth of approximately 20 m beneath the land surface (Figure 2). The overall dimensions of the model domain are 30 m depth, 250 m width, and 1075 m length. A grid was developed using the TOUGH2 grid generator, Wingridder (Pan, 2003), that had finer resolution near the wells such that the nine pipes could be modeled (Figure 3). A

constant river width of 60 m was used, and no bends in the river were modeled since this section of the river is relatively straight. A streambed with a uniform thickness of 1 m and a slope of 0 was used; spatial variability in the river depth was not incorporated into the model. The river depth was modeled as a constant pressure boundary condition with a head of 1.2 m since this portion of the river is in the backwater of the inflatable dam, and the river depth remains nearly constant over time when the dam is raised. Such an approximation worked well for two-dimensional modeling of heat transport from the stream to adjacent observation wells along the Russian River (Su et al., 2004).

The bottom of the model and the boundaries on the east and west sides were the approximate locations of the bedrock contact and were therefore considered no flow boundaries. The distance to the bedrock boundaries on the bottom and the east and west sides of the model domain were estimated by SCWA using geologic maps, logs from borings, and geophysics. In the simulations, the distances to the bedrock boundaries are uniform and represent the average distance to those boundaries over that reach of the river. Constant pressure head boundaries were used on the north and south sides of the model, such that the pressure difference across the model domain resulted in a hydraulic gradient of 0.001 and groundwater flow occurred from north to south.

The air and water phases were modeled separately in the simulations (Pruess, 2004). An air mass fraction of 1 and a gas pressure of 1×10^5 Pa were applied the top of the domain to provide the boundary condition for the air phase. The aquifer was saturated before the simulations began and the initial water table was at the level of the streambed ($z = 24$ m). The initial moisture content in

the unsaturated zone was obtained by allowing the soil to equilibrate with a water table at $z = 24$ m.

A total of 22 layers were used in the simulations with thicknesses that ranged from 1 to 2 m, except for a layer with a thickness of 0.2 m at the depth of the 0.2 m-diameter laterals. The streambed was also modeled as a separate layer with a thickness of 1 m. When the permeability of the streambed was changed, the entire streambed layer was assigned that permeability with the exception of the simulations conducted in Case 3, where a rectangular region was placed in the streambed center near the collector wells that had a lower permeability compared to the rest of the streambed. The lower permeability layer has a width of 13 m and a length of 250 m and was placed in the bottom 0.5 m of the streambed layer. This scenario was modeled because estimates of streambed fluxes by Gorman (2004) and Constantz et al. (2006) in the region near the collector wells indicated larger fluxes along the east and west river banks compared to the center of the stream. Some researchers have demonstrated that a lower permeability streambed layer may not be present in a stream-aquifer system (e.g., Cardenas and Zlotnik, 2003; Kollet and Zlotnik, 2003). The reach of the Russian River that we are simulating in this study is in the backwaters of an inflatable dam, where deposition of fine-grained sediment along the streambed occurs, resulting in a streambed layer that has a permeability lower relative to the aquifer permeability.

In all the simulations, the two wells each pumped continuously at a rate of $1600 \text{ m}^3/\text{hr}$ (10 mgd) for a total rate of $3200 \text{ m}^3/\text{hr}$. This was the average pumping rate for the two collector wells during the summer to fall months of 2003 when the inflatable dam was raised. The average

length of the laterals, 35 m, was used as the length for each of the laterals in the model. The total pumping rate for the collector wells was divided uniformly over all the laterals; therefore, each lateral was assigned a pumping rate of 178 m³/hr. The pumping rate for each lateral was then divided uniformly by the number of nodes representing the lateral. The configuration of the laterals is based on their actual orientation. Internal head losses and skin effects along the laterals are not considered in these simulations; Bakker et al. (2005) developed an analytic element method that accounts for these effects.

The streambed permeability values used in the simulations are in the range of permeabilities estimated along the Russian River by Gorman (2004) and Su et al (2004). Streambed permeabilities (hydraulic conductivities) estimated by Gorman (2004) in June and September 2003 for the areas near the Bank Filtration Facility ranged from 1.4×10^{-12} to 2.6×10^{-11} m² (1.4×10^{-5} m/s to 2.6×10^{-4} m/s). The best fit effective permeability (hydraulic conductivity) based on inverse modeling of temperature profiles in those same locations (Su et al, 2004) ranged from 5.5×10^{-12} to 2.0×10^{-11} m² (5.5×10^{-5} to 2.0×10^{-4} m/s). Permeabilities measured from pumping tests ranged from 2.4×10^{-10} to 6.5×10^{-10} m² (2.4×10^{-3} to 6.5×10^{-3} m/s). The pumping tests provide an estimate of the permeability of only the aquifer, whereas the permeability estimated using the temperature profiles gives an effective permeability of both the streambed and aquifer. Therefore, the values estimated from the pump tests were assumed to be representative of the aquifer permeability since the permeability of the streambed layer was not incorporated in the estimates from the pumping tests. A permeability of 2.4×10^{-10} m² was used as the aquifer permeability in Cases 1, 3, and 4. A slightly lower value of 7.4×10^{-11} m² was used in Case 2. The streambed and aquifer conductivity was assumed isotropic in all the simulations except for

Case 4 where an anisotropy of five was used to investigate the effect of anisotropy on the development and extent of the unsaturated region. In this case, only the aquifer was considered to be anisotropic, and the streambed was still considered to be isotropic. Su et al (2004) found that an anisotropy of five gave the best fit when simulating groundwater temperature profiles along the Russian River.

The van Genuchten function (van Genuchten, 1980) was used in the simulations to describe the characteristic curves of the streambed and aquifer. Characteristic curves of the porous material along the Russian River have not been measured; therefore, parameters for the van Genuchten function were obtained from Carsel and Parrish (1988). Parameters measured for sand were used for the aquifer and parameters measured for silt were used for the streambed. A porosity of 0.35 was used for both the silt and sand. A summary of the parameters used in the simulations is presented in Table 1.

The three-dimensional TOUGH2 model is used to conduct a simulation analysis of the formation of an unsaturated region beneath the streambed and to evaluate the sensitivity of well production as the streambed and aquifer hydraulic properties change. Although this model is based on the SCWA facilities and the permeabilities of the streambed and the aquifer are in the range of the field estimates of that region, the model developed was not calibrated with point measurements taken in the streambed and aquifer (e.g., temperature and pressure). This will be performed in a future phase of this study when more field data is available. The effect of the different aquifer to streambed permeability ratios on the flow velocities through the streambed is also examined in our simulations and compared with field measurements. To quantify travel times of the stream

water reaching the collector wells, simulated breakthrough curves of a conservative tracer continuously released into the stream are obtained at the collector wells over a period of 30 days. The tracer concentrations at both wells are averaged in the simulated breakthrough curves. Four simulation cases were conducted and the streambed and aquifer permeabilities used in the different cases are summarized in Table 2.

3. RESULTS

3.1. Water Saturation Beneath the Streambed and Between the Collectors Well

Installation of shallow piezometers confirmed the existence of an unsaturated zone beneath the streambed at relatively shallow depths (2 meters) in some locations near the collector wells. Monitoring unsaturated conditions below a river is challenging and only limited data is available. Piezometers were installed recently fitted with tensiometers and with time domain reflectometers to measure water content (Su et al., 2006). Monitoring results indicated negative pore pressures and water contents less than saturated values at depths ranging from 0.9 m to 2.4 m. Simulations were run to determine the streambed and aquifer permeability characteristics that could create these unsaturated conditions.

3.1.1. Effect of different streambed and aquifer permeabilities

Over the 30-day period that the simulations were run under continuous pumping, the aquifer beneath the streambed remained saturated and was under positive pressure when the aquifer and

streambed permeabilities were the same (both $2.4 \times 10^{-10} \text{ m}^2$), and when the streambed permeability was lowered by an order of magnitude such that the aquifer to streambed permeability ratio was 10 (Cases 1a and 1b, respectively). In Case 1c, where the aquifer to streambed permeability ratio was 100, an unsaturated region beneath the streambed in Case 1c began to form within 30 minutes of continuous pumping. The unsaturated region first formed near the east bank of the river and then progressed westward over time and reached an equilibrium size beneath the streambed within 10 hours after pumping began. The steady-state size of the unsaturated region beneath the streambed had dimensions of 25 m width from the east bank of the river, 130 m length, and depth of 3 m. Figure 4 contains plots of the saturation beneath the streambed and in the aquifer after 7 days of continuous pumping. Additional drawdown of the water table occurred in the aquifer east of the riverbank over time, but the unsaturated region beneath the streambed was at an equilibrium state caused by the low streambed permeability. The size of the unsaturated region would be altered if changes in the streambed permeability and pumping rate occurred over time, but these simulations are conducted with a constant permeability and pumping rate.

The extent of the region with pressures less than atmospheric (101,325 Pa) in Case 1c was larger than the unsaturated region and extended completely across the river (Figure 4). Therefore, it is possible for much of the region beneath the streambed to be saturated, but to be under negative pressure (relative to atmospheric pressure) during pumping because the air entry pressure of the aquifer material has not yet been reached. Both an unsaturated region and a saturated region under negative pressure would be indicated by dry piezometers, as has been observed near the two collector wells along the Russian River.

In Case 1d, the streambed permeability is $7.4 \times 10^{-13} \text{ m}^2$, which is 2.5 orders of magnitude less than the aquifer permeability. Plots of the liquid saturation in the aquifer after 7 continuous days of pumping in Figure 5 show that a large unsaturated region formed beneath the river that extended entirely across the river, had a length of 425 m, and a maximum depth of 8 m. The pressure beneath the streambed is plotted next to the saturation in Figure 5 and shows a negative pressure region that is still saturated because of the air entry pressure of the aquifer material. This region exists about 50 m upstream and downstream from where the unsaturated region ends. In this case, the size of the unsaturated region beneath the streambed was not at steady-state after 7 days of continuous pumping. It continued to increase over time until the simulation stopped running after 12.5 days because the aquifer near the wells desaturated and water could no longer be produced at a rate of $3200 \text{ m}^3/\text{hr}$. The desaturated region had a maximum length of 470 m, width of 60 m, and depth of 13 m when the simulation stopped. This result has important implications for well operation. During the summer and fall months when the inflatable dam is raised and portions of the streambed permeability decrease over time because of the accumulation of fines along the streambed, the well operation may have to be altered if the permeability decreases to a value where a large unsaturated region forms in the aquifer. The collector wells may have to be shut off for periods of time so the formation can resaturate. Based on the conditions used in the simulations, the threshold streambed permeability where the aquifer desaturates significantly beneath the streambed occurs over a relatively narrow range between 7.4×10^{-13} and $2.4 \times 10^{-12} \text{ m}^2$.

The results from Case 1d in Figure 5 show that the boundaries on the east and west side of the domain where the bedrock contact is located has an impact on the configuration of the unsaturated region that develops. If the domain is larger in those directions, the unsaturated region would extend further out on the east and west sides and the extent of the unsaturated region along the north-south direction would decrease. The range of streambed permeabilities over which the pumping capacity could be sustained would also increase with a larger domain since more aquifer storage would be available. Case 1d was also run using a longitudinal head gradient of 0.003 instead of 0.001. The threshold permeability ratio where pumping was no longer sustained remained the same; however, the time at which the pumping rate could not be sustained occurred two days later compared to when the gradient was 0.001.

In Case 2a, the aquifer beneath the streambed remained saturated when the aquifer and streambed permeabilities were the same at $7.4 \times 10^{-11} \text{ m}^2$ over the 30-day simulation run. For a streambed permeability of $7.4 \times 10^{-12} \text{ m}^2$ and an aquifer permeability of $7.4 \times 10^{-11} \text{ m}^2$ (Case 2b), a narrow unsaturated region developed adjacent to the east bank and reached its equilibrium size within 24 hours after pumping began. The maximum dimensions of the steady-state unsaturated region below the streambed were 5 m width, 120 m length, and 3m depth. When the streambed permeability decreased to $5 \times 10^{-12} \text{ m}^2$ in Case 2c, an equilibrium unsaturated region also developed beneath the streambed within 24 hours after pumping began and had a maximum length of 130 m, a width of 16 m, and a depth of 3 m. In Case 2d, which had a streambed permeability of $2.4 \times 10^{-13} \text{ m}^2$, the size of the unsaturated region beneath the streambed increased over time until reaching a maximum dimension of 160 m length, 40 m width, and 13 m depth

after 2.5 days of continuous pumping. The simulations stopped at this time because water could no longer be produced from the wells at a rate of $3200 \text{ m}^3/\text{hr}$.

The results from Cases 1 and 2 demonstrate that as the aquifer permeability decreases, the unsaturated region beneath the streambed develops at a smaller aquifer to streambed permeability ratio. For the two aquifer permeabilities used in the simulations, the aquifer to streambed permeability ratio where the unsaturated region developed was around 100 for the larger aquifer permeability and only 14 for the lower aquifer permeability. In addition, the range of streambed permeabilities over which the aquifer is unsaturated, but water can still be produced at a rate of $3200 \text{ m}^3/\text{hr}$ decreases as the aquifer permeability decreases. Below a critical permeability, the water table in the aquifer is lowered so drastically over a relatively short time period that the pumping rate can no longer be sustained. These results are specific for the system modeled in this paper. Many factors can impact these results including the extent of the domain boundaries, pumping rate, aquifer and streambed heterogeneities, and location and depth of the laterals relative to the river.

3.1.2. Effect of non-uniform streambed permeability

To investigate how non-uniformity in the streambed permeability affects the development of the unsaturated region, a lower permeability region was placed in the center of the streambed in Case 3. Figure 2 shows the location of the lower streambed permeability region. This region was placed along the lower 0.5 m of the streambed rather than over the entire streambed depth since field observations indicate that this lower permeability layer may begin at some depth beneath

the top of the streambed (D. Rosenberry, USGS, personal communication). The depths over which this lower permeability layer exists have not yet been identified, however. When the lower permeability region of the streambed is $2.4 \times 10^{-12} \text{ m}^2$ while the remainder of the streambed has a permeability of $2.4 \times 10^{-11} \text{ m}^2$, the aquifer beneath the streambed remains saturated. The water saturation beneath the streambed when the lower permeability portion of the streambed is $2.4 \times 10^{-13} \text{ m}^2$ while the remainder has a permeability of $2.4 \times 10^{-12} \text{ m}^2$ is shown in Figure 6 after 7 days of continuous pumping. The size of the unsaturated region beneath the streambed is at equilibrium in this case with maximum dimensions of 160 m length, 60 m width, and 7 m depth. The region beneath the lower permeability portion has a lower saturation compared to the regions around it. The pressure distribution beneath the streambed is shown next to the saturation plot and shows that a 20 m long negative pressure region that is saturated exists upstream and downstream of where the unsaturated region ends. While this study is not focused on an extensive investigation of the effect of streambed heterogeneities on the water saturation beneath the streambed, the results of the simulations from Case 3d compared to Case 1c demonstrate the importance of the streambed permeability distribution on the development of an unsaturated region and the resulting water saturation beneath the streambed. In Case 1c, where the streambed is uniform and has a permeability of $2.4 \times 10^{-12} \text{ m}^2$, the maximum width of the unsaturated region at an equilibrium state is 25 m whereas it extends entirely across the river (60 m) in Case 3d. The length of the unsaturated region is slightly larger in Case 3d compared to Case 1c and the depth in those two cases are the same.

The impact of heterogeneities in the streambed on the exchange between stream water and the streambed has been examined in a number of studies (e.g., Cardenas et al., 2004; Salehin et al.,

2004; Ryan and Boufadel, 2006). Many researchers have also demonstrated the importance of heterogeneities on flow and transport through the subsurface in alluvial environments (e.g., Weissmann et al., 2000; LaBolle et al. , 2006). Heterogeneities give rise to preferential pathways, where faster flow occurs through regions with higher permeabilities. Cardenas et al. (2004) found that exchange between the stream water and streambed is dominated by streambed heterogeneities when the head variation is small. Salehin et al. (2004) investigated exchange in heterogeneous sand beds and observed a shallower zone with higher rate of exchange when there was heterogeneity. Ryan and Boufadel (2006) conducted tracer tests along a small urban stream to quantify the exchange of stream water with shallow sediments. They observed high tracer concentrations when the upper streambed layer had a larger permeability than the layer below it.

Currently, only limited data on the streambed permeabilities along the Russian River are available, but when additional measurements are made in the future, simulations should be performed to investigate how the pumping capacity at the collector wells would be affected by a heterogeneous streambed and aquifer with an average permeability equal to the permeabilities from the homogeneous case. Heterogeneities in the streambed permeability will also affect the water saturation of the desaturated region beneath the streambed, where higher saturations are expected below regions with lower streambed permeability. The depth of the unsaturated region will also be impacted by the streambed permeability. For a particular distance away from the collector well, the depth of the unsaturated region will be greater below a region of lower streambed permeability compared to a region of higher permeability.

3.1.3. Effect of Anisotropy Ratio

In Case 4a, simulations were run under the same conditions as Case 1c except that an anisotropy ratio of 5 was used for the aquifer instead of 1. The anisotropy ratio in the streambed remained as 1 in these simulations. An unsaturated region developed beneath the streambed with an equilibrium size similar to that of Case 1c (see Table 2). However, the saturation in the unsaturated region is greater when an anisotropy ratio of 5 was used compared to a ratio of 1. The unsaturated region in the aquifer east of the river also extends further east for an anisotropy of 5. In Case 4b, the same conditions as Case 1d were used except an anisotropy ratio of 5 was used for the aquifer. The saturation in the unsaturated regions of the aquifer was once again higher when the formation was anisotropic compared to when it was isotropic. However, the simulation stopped running after 7.8 days in Case 4b instead of 12.5 days as in Case 1d. Therefore, even though the water saturation of the unsaturated region was smaller when the aquifer was isotropic, the recharge rate from the stream into the aquifer was greater in the isotropic case because of the larger vertical permeability. The region was dewatered at a slower rate in the isotropic case compared to the anisotropic case and production of water at 3200 m³/hr could be maintained for a longer period. Streambed heterogeneity, which was not considered in this study, can lead to an effective anisotropy that limits penetration (Salehin et al., 2004). This would reduce the recharge rate from the stream into the aquifer and likely decrease the period over which water can be produced at a particular rate.

3.2. Measured and Simulated Velocities Along the Streambed

Streambed velocities in the vicinity of the two collector wells were estimated by Gorman (2004) using seepage meters and by Contantz et al. (2006) using surface and groundwater temperature profiles and are presented in Figure 7. Seepage meters are more difficult to operate in streams than lakes, but if the seepage bag is protected from streamflow currents (as was done by Gorman, 2004), seepage meter reading in streams can be as reliable as measurements in lakes. Gorman (2004) measured velocities at two cross-sections near the collector wells while Contantz et al. (2006) obtained velocities at three cross-sections. At each location, the velocities were measured across the stream at three points: one near the east bank (where the collector well resides), one near the west bank, and one in the center of the stream. The changes in the velocities measured by Gorman (2004) during June 2003 and then September 2003 at the two locations demonstrate that the velocities change during the period that the dam was raised. In the vicinity of the collector wells and downstream of the wells, the velocities on the east and west bank are higher compared to the center, with the velocities on the east bank generally higher than the velocities on the west. This is expected since some of the laterals from the collector wells extend underneath the streambed on the east side. However, a trend of increasing velocities from the west to east bank is also observed upstream of the collector wells, suggesting that sediment scour and depositional pattern may also contribute to the west to east trend.

Plots of the simulated pore velocities beneath the river at a location between the collector wells ($Y = 540$ m) are shown in Figure 8. Figures 8a - 8c and Figures 8d - 8f show the velocity plots at 0.25 m and 2 m, respectively, beneath the river for Cases 1 - 3. The plots at 0.25 m beneath are in

the streambed while the plots at 2 m beneath are in the aquifer. The negative values for the velocities are used so that they follow the convention used in the measured values. For Cases 1a and 1b, the velocities increase non-linearly from the east to west bank. Even though the streambed permeability is an order of magnitude larger in Case 1a versus 1b, the velocities from Case 1b are actually higher across the river, except for the region next to the east bank where the velocities in Case 1a increase dramatically and are much larger than in Case 1b. Because such a high velocity is obtained on the east side in Case 1a, the velocities along the rest of the stream are smaller compared to Case 1b since those velocities in addition to the velocities on the east side are large enough to sufficiently recharge the aquifer. In Case 1c, where the streambed permeability is two orders of magnitude smaller than the aquifer permeability, the velocities in the streambed (0.25 m beneath the river) increase slightly from the west to east bank. At 2 m beneath the river, the velocities steadily increase from the west to east bank from $x = 40$ to 60 m, but then they decrease from $x = 60$ to 85 m and are nearly constant from $x = 85$ to 100 m. The change in the velocity profile in Case 1c compared to Case 1a and 1b is because an unsaturated region has formed beneath the streambed in Case 1c and the velocities on the east side are reduced because the aquifer is unsaturated. From the water saturation profiles shown in Figure 4, the unsaturated region extends a maximum distance of around 25 m from the east bank. The maximum velocity beneath the streambed occurs around 33 m from the east bank which is just beyond where the formation is saturated again.

The magnitude of the velocities for Cases 1a and 2a are nearly the same. Even though the streambed and aquifer permeabilities are less in Case 2a compared to Case 1a, the pore velocities beneath the river are still the same in both cases. The velocities in Case 2b are smaller towards

the east bank compared to Case 1b because the seepage rate had been sufficiently reduced by the lower streambed permeability and an unsaturated region developed. The velocities across the river in Case 2c are consistently higher than Case 1c, but the streambed permeability in Case 2c was greater than in Case 1c.

The measured trend in streambed velocities where the velocities in the center of the stream are smaller than the velocities along the east and west banks (Figure 7) was not reproduced in the simulated results from Cases 1 and 2. In fact, the opposite trend is observed in Case 1c where the simulated velocities are highest in the center. The field measurements suggest that the streambed permeability is not uniform; therefore, simulations conducted in Case 3 are used to investigate whether the presence of a lower permeability region near the center could reproduce the measured trend. The velocity profiles across the stream from Case 3 are shown in Figures 8c and 8f. The velocity trend from this case is similar to the trend observed in the measured velocities where a lower velocity in the center of the stream is observed relative to the east and west bank.

Permeabilities were also estimated by Gorman (2004) from grain size analyses of streambed sediment samples at the same locations where the velocities were measured. The estimated permeabilities in the center were not significantly lower, or in some cases were even larger, than the permeabilities measured on the east and west bank. As mentioned earlier, the lower permeability streambed layer is likely located at some depth beneath the streambed surface. Therefore, the streambed permeabilities estimated by Gorman (2004) may have only been representative of the upper portion of the streambed where the permeability is larger. Streambed

velocities are affected by the presence of the lower permeability layer in the lower half of the streambed, as demonstrated by the simulations in Case 3 shown in Figure 8c.

3.3. Simulated Volumetric Streambed Fluxes

The simulated velocities at each grid node immediately beneath the stream were multiplied by the corresponding grid block area and then summed together to obtain the total volumetric streambed fluxes from the different cases that are presented in Table 2. This depth was chosen because the majority of the water is entering vertically at this depth. In the cases where the pumping rate was sustained, the fluxes after seven days of continuous pumping range from 2500 to 3100 m³/hr, which is 78 to 97% of the total flow rate produced at the collector wells. Only a small change in the total streambed flux occurred over time. For instance, in Case 1c, the streambed flux increased very slightly after 1 day compared to 28 days of continuous pumping, from 90 to 92% of the total flow rate produced at the collector wells. Figure 9 contains a plot of the total streambed flux normalized by the pumping rate over time for Cases 1d and Cases 4b, two of the cases where the production rate at the well could not be sustained. The streambed flux increases slightly over time in those 2 cases before production at the well could no longer be sustained, varying between 41 to 47% of the total rate produced at the well. For the cases where the pumping rate was sustained, the normalized fluxes at the upstream (north) and downstream (south) boundaries of the model domain are also summarized in Table 2. The fluxes at those boundaries range from 0.1 to 5% of the total flow rate produced at the well.

No consistent trend in the change in volumetric flux occurs as the streambed permeability decreases in the different cases. The volumetric streambed flux from Case 1b is higher than 1a, but Case 1c is lower than 1b. The fluxes on the eastern half of the streambed are lower in 1b compared to 1a but the fluxes on the western half are higher in 1b. The fluxes on the western side are large enough that the overall streambed flux is greater compared to 1a. In 1c and 1d, the lower streambed permeability reduces the streambed flux relative to Case 1b. In Case 2, the streambed fluxes increase as the streambed permeability decreases from 2a to 2c, even though an unsaturated region is present. This is because the streambed permeability is not small enough in those cases to produce an unsaturated region that is large enough to reduce the overall flux as in Cases 1c and 1d. The streambed fluxes also increase on the western side as the permeability decreases. In Case 3, a slightly lower streambed flux is obtained for Case 3b compared to 3a. Compared to 3a, the fluxes in Case 3b are slightly higher on the eastern side, higher on the western side, but lower in the center where the lower permeability streambed region is. In Case 3c, the streambed fluxes on the western side of the river are larger compared to 3a and 3b, but smaller on the eastern side; however, the sum of the total flux over the entire streambed is greatest in 3c. A smaller flux is observed in 3d because the lower permeability streambed results in reducing the overall streambed flux.

3.4. Stream Water Travel Times to the Collector Wells

A series of simulations were run to obtain quantitative information on the travel times of the stream water reaching the wells by continuously releasing a conservative tracer into the stream for 30 days. A cumulative breakthrough curve (BTC) of the average tracer concentration at the

two collector wells was obtained for Cases 1 – 3, and the results are presented in Figure 10. As the streambed permeability decreases, the travel times of the tracer reaching the wells increase and the tracer concentration at the well decreases. The breakthrough curves for some of the cases overlap with each other. For instance, Cases 1a and 1b overlap with Cases 3a and 3c, respectively. In Cases 3a and 3c, the permeability in the center is one order of magnitude smaller than the permeability in the remainder of the streambed. Therefore, the lower permeability layer in Cases 3a and 3b did not have much impact on the breakthrough curves compared to when the streambed was uniform, although the flow velocities near the streambed were affected by the lower permeability layer. However, when the permeability of the center layer was reduced to $2.4 \times 10^{-13} \text{ m}^2$ while the remainder of the streambed was at $2.4 \times 10^{-12} \text{ m}^2$, the tracer travel times were significantly reduced compared to the case where the streambed was uniform at $2.4 \times 10^{-12} \text{ m}^2$.

The ratio between the tracer concentrations at the wells to the initial tracer concentration does not ever approach 1 in any of the cases after 30 days. In Cases 1a, 2a, 3a, and 3b, the concentration at the well nearly levels off after 30 days while in the remaining cases the concentration still increase with time. The concentration of the tracer at the well can also be used to approximate the mixing ratio between the stream water and groundwater at the collector wells. Assuming that the stream and groundwater are well-mixed at the well, the concentration of tracer at the well, C_{well} , can be written as

$$\frac{C_{well}}{C_0} = \frac{[C_0 V_{stream} + C_{gw} V_{gw}]/V_{stream+gw}}{C_0} \quad (1)$$

where C_0 is the concentration of solute in the stream, C_{gw} is concentration of solute in the groundwater, V_{stream} is the volume of water from the stream collected at the well, V_{gw} is the volume of water from the groundwater collected at the well. $C_{gw} = 0$ in the simulations, therefore Equation (1) becomes

$$\frac{C_{well}}{C_0} = \frac{[C_0 V_{stream}] / V_{stream+gw}}{C_0} = \frac{V_{stream}}{V_{stream+gw}} \quad (2)$$

The fraction of the water collected at the well that originates from the stream is therefore proportional to C_{well}/C_0 . In the simulations we assume that all the water initially in the aquifer before pumping occurs is groundwater. Information on the actual fraction of the water from the stream versus the groundwater is not available for this site, but these simulations provide a general trend as to how the fraction of stream water collected at the wells changes as aquifer to streambed permeability ratio changes. From the breakthrough curves in Figure 10, the fraction of the water from the stream decreases as the streambed permeability decreases, which occurs because the lower streambed permeability reduces the flux of stream water into the aquifer and more of the water extracted is groundwater in order to produce at the same rate. After 30 days, the ratio of streambed water to groundwater ranges from 0.6 to 0.9 for the different simulation scenarios.

Solute transport simulations were also conducted in Case 2b to investigate the differences in travel times of the stream water originating from the west side versus the east side and the differences in the fraction of the stream water that reaches the wells. Tracer was only introduced on the western half of the stream ($x = 40$ to 70 m) and similarly over the eastern half ($x = 70$ to

100 m) to obtain the stream travel times of the different sides. The results shown in Figure 10c demonstrate that the travel times on the western side of the stream are, as expected, slower than the ones from the eastern side. In addition, a smaller percentage of the stream water from the western half of reaches the aquifer near the wells, around 25% compared to 55% for the eastern side after 30 days of continuous pumping.

The solute transport simulations demonstrate that the fraction of stream water collected at the wells is less than one in all the cases, indicating that not all of the water that leaves the streambed recharges the aquifer around the wells. In the cases where the total streambed flux becomes higher as the streambed permeability becomes lower (see Table 2), the fraction of stream water that reaches the wells decreases. Therefore, for the conditions simulated in this study, a higher streambed flux does not necessarily indicate greater recharge to the region around the wells.

4. CONCLUSIONS

The complex hydrology beneath a stream with an adjacent groundwater pumping facility requires a comprehensive, physically based simulation model to properly characterize the hydraulics and residence time within the system. A detailed three-dimensional multi-phase flow and transport model was successfully constructed using TOUGH2 to simulate the extent of the unsaturated region beneath the streambed of the Russian River, and to examine the sensitivity of these kinds of system when the aquifer to streambed permeability ratio changes. The 3-D model developed in this study was based on the Russian River Bank Filtration Facility in Sonoma County, California where two horizontal collector wells are located near the riverbank.

Limitations on the model developed are that the streambed topography was not included in the simulations and the river was approximated as having a constant width and modeled as a constant pressure boundary condition. Streambed topography could have a significant influence on near shallow-stream flows, which were not considered in this study. The bedrock contacts on the east and west sides and the bottom of the simulation domain were also modeled with uniform distances. Another limitation of this model is that the streambed and aquifer were simulated as homogeneous layers. Future research is warranted to investigate the impact of heterogeneities along the streambed and in the aquifer since they affect stream-groundwater interactions and travel times to the wells. For the purposes of evaluating the impact of the aquifer to streambed permeability ratio on pumping-induced unsaturated regions beneath a river and on travel times, the model developed contains many of the key components for investigating how the SCWA facility responds as the permeability ratio changes.

The simulations demonstrate that as the ratio between the aquifer to streambed permeability increases, the size of the unsaturated region beneath the streambed is predicted to increase. The threshold aquifer to streambed permeability ratios at which the unsaturated region was first observed ranged between 10 to 100 for the conditions simulated in this study. The simulations also indicated that for a particular aquifer permeability, decreasing the streambed permeability by only a factor of 2 - 3 from the permeability where desaturation initially occurred resulted in a reduction in the pumping capacity. These results may be specific for the unique boundaries that occur along the reach of the Russian River that was modeled in this study. For instance, the range of aquifer to streambed permeabilities over which the well production is not impacted

would be greater if the distance to the boundary on the east and west sides increased because of larger storage in the aquifer. These simulations demonstrate that a three-dimensional, multiphase flow and transport model is a useful tool in planning the location of horizontal collector wells because site specific constraints could have a large impact on the production rate. Temporal changes in the streambed permeability are also very important to consider in addition to the spatial variability. For the Russian River, these results have significant implications on management of the collector wells during the summer to fall months when the dam is raised and the permeability decreases over time.

Measured seepage meter and temperature-based streambed velocities near the collector wells indicate that the velocities along the center of the Russian River are often lower than the fluxes on the east and west banks. When the streambed is modeled as a homogeneous layer and the aquifer beneath is saturated, the simulations show that the streambed velocities increase across the channel, with the largest velocities on the east bank near the collector wells. Because the pattern of the measured streambed velocities was not reproduced when the streambed was homogeneous, simulations were conducted with a lower permeability layer placed in the center of the streambed. In this case, the velocity pattern observed in the field measurements was qualitatively reproduced in the simulations.

A simulated conservative tracer was released continuously into the stream to obtain the breakthrough curves at the collector wells, providing a quantitative comparison of the residence time of the water originating from the stream for different streambed permeabilities. Knowledge of these residence times is important for optimizing the effectiveness of filtration while

maintaining saturated conditions beneath the streambed. In our simulations, the percentage of tracer at the well was proportional to the amount of stream water at the well. As the streambed permeability decreased, the percentage of stream water at the well decreased and more groundwater was needed to sustain the pumping rate.

No consistent trend was observed in the change in total volumetric streambed flux as the streambed permeability decreased in the different cases. In some cases, the total flux even increased as the streambed permeability decreased because the fluxes on the western side of the streambed were higher. However, the percentage of stream water that reached the collector wells decreased as the streambed permeability decreased. Therefore, for the system simulated in this study, the magnitude of the streambed flux does not correlate to the rate at which the stream recharges the region around the collector wells.

Numerical simulations also play an important role in site characterization in near-stream environments because they can be used to make decisions on the type of data to collect, the important regions to focus characterization efforts on, and the scale over which measurements should be made. An iterative process between modeling and data collection should be used since extensive characterization of a site is difficult and expensive. Preliminary characterization of the desaturated region below the river that was modeled in this study has been made using tensiometers, temperature sensors, and water content sensors (Su et al., 2006). These measurements provide important data on surface-groundwater interactions and the unsaturated region that can subsequently be used to calibrate the numerical model. In addition, geophysical techniques such as ground penetrating radar and electrical resistivity tomography have been

evaluated near our study site and show potential for imaging cross-sections of the desaturated region below the river.

5. ACKNOWLEDGMENTS

This work was supported by the Sonoma County Water Agency (SCWA), through U.S. Department of Energy Contract No. DE-AC03-76SF00098. Thanks are due to Christine Doughty (LBNL) for helpful discussions on setting up the TOUGH2 simulations, and to Curt Oldenburg (LBNL), Aaron Packman (Northwestern University), and three anonymous reviewers for reviewing this manuscript. Also, appreciation goes to Marisa Cox and Donald Rosenberry (U.S. Geological Survey), Peter Gorman (PES, Inc.), and Christine Hatch (U.C. Santa Cruz) for making their data and understanding of the system available to the authors.

6. REFERENCES

- Anderson, M.P. (2005), Heat as a Ground Water Tracer, *Ground Water*, 43(6), 959-968.
- California Department of Water Resources (1983), Evaluation of ground water resources: Sonoma County, Volume 5, Alexander Valley and Healdsburg Area.
- Bakker, M., V. A. Kelson, and K. H. Luther, Multilayer analytic element modeling of radial collector wells, *Ground Water*, 43(6), 926-934, 2005.
- Cardenas, M.B.R. and V.A. Zlontik (2003), Three-dimensional model of modern channel bend deposits. *Water Resour Res* 2003;39(6):1141. doi:10.1029/2002WR001383.
- Carsel, R.F. and R.S. Parrish (1988), Developing joint probability distributions of soil water retention characteristics, *Water Resour. Res.*, 24(5), 755-769.
- Constantz, J., M.H. Cox, and G.W.Su (2003), Comparison of heat and bromide as ground water tracers near streams, *Ground Water*, 41(5): 647-656.
- Constantz, J., G.W. Su, and C. Hatch (2006), Heat as a ground water tracer at the Russian River RBF facility, Sonoma County, California, *Riverbank Filtration Hydrology*, edited by S. A. Hubbs, pp. 243-259, Springer Publ., Dordrecht, The Netherlands.
- Cox, M.H., G.W. Su, and J. Constantz (2007), Heat, chloride, and specific conductance as groundwater tracers near streams, *Ground Water*, 45(2): 187-195.
- Fox, G.A. and D.S. Durnford (2003), Unsaturated hyporheic zone flow in stream/aquifer conjunctive systems, *Advances in Water Resources*, 26, 989-1000.
- Gorman, P.D. (2004), Spatial and temporal variability of hydraulic properties in the Russian River streambed, Central Sonoma County, California, M.S. Thesis, San Francisco State University, San Francisco, California.

- Greskowiak, J., H. Prommer, G. Massmann, C.D. Johnston, G. Nützmann, A. Pekdeger (2005), The impact of variable saturated conditions on hydrogeochemical changes during artificial recharge of groundwater, *Applied Geochemistry*, 20, 1409-1426.
- Hunt, B. (1999), Unsteady stream depletion from ground water pumping, *Ground Water*, 37 (1): 98-102.
- Hunt, R.J., T.B. Coplen, N.L. Haas, D.A. Saad, and M.A. Borchardt (2005), Investigating surface water-well interaction using stable isotope ratios of water, *J. of Hydrology*, 302, 154-172.
- Kollet S.J. and V.A. Zlotnik (2003), Stream depletion predictions using pumping test data from a heterogeneous stream-aquifer system (a case study from the Great Plains, USA). *J of Hydrology*, 281, 96-114.
- LaBolle, E.M., G.E. Fogg, J. Gravner, and J.B. Eweis (2006), Diffusive fractionation of ^3H and ^3He and its impact on groundwater age estimates, *Water Resour. Res.*, 42, W07202, doi:10.1029/2005WR004756.
- Ryan, R.J. and M.C. Boufadel (2006), Influence of streambed hydraulic conductivity on solute exchange with the hyporheic zone, *Environ. Geol.*, DOI 10.1007/s00254-006-0319-9.
- Rosenberry, D.O. (2000), Unsaturated-zone wedge beneath a large, natural lake, *Water Resour Res.*, 36(12), 3401-3409.
- Pan, L. (2003), Wingridder — An interactive grid generator for TOUGH2, Proceedings, TOUGH Symposium 2003, Lawrence Berkeley National Laboratory, Berkeley, California, May 12 - 14, 2003.
- Pruess, K., C.M. Oldenburg, and G. Moridis (1999), TOUGH2 user's guide, version 2.0: Berkeley, CA, Lawrence Berkeley National Laboratory Report LBNL-43134.

- Pruess, K. (2004), The TOUGH Codes—A Family of Simulation Tools for Multiphase Flow and Transport Processes in Permeable Media, *Vadose Zone Journal*, 3:738-746.
- Reid, M. E., and S. J. Dreiss (1990), Modeling the effects of unsaturated, stratified sediments on groundwater recharge from intermittent streams, *J. Hydrology*, 114, 149-174.
- Salenhin, M. A.I. Packman, and M. Paradis, Hyporheic exchange with heterogeneous streambeds: laboratory experiments and modeling, *Water Resources Res.*, 40, W11504, DOI:10.1029/2003WR002567.
- Schubert, J. (2002), Hydraulic aspects of riverbank filtration—field studies. *Journal of Hydrology*, 266, 145-161.
- Sheets, R.A., R.A. Darner, and B.L. Whitteberry (2002), Lag times of bank filtration at a well field, Cincinnati, Ohio, USA, *Journal of Hydrology* 266, 162-174.
- Stonestrom, D.A. and J. Constantz (2003), Heat as a tool for studying the movement of ground water near stream, U.S. Geological Survey Circular 1260.
- Su, G.W., J. Jasperse, D. Seymour, and J. Constantz (2004), Estimation of hydraulic conductivity in an alluvial system using temperature, *Ground Water*, 42(6): 890-901.
- Su, G.W., J. Jasperse, D. Seymour, J. Constantz, C. Delaney, and Q. Zhou (2006), Pumping-induced unsaturated regions beneath a perennial river, *Eos Trans. AGU*, 87(52), Fall Meet. Suppl., Abstract H11A-1223.
- van Genuchten, M.T. (1980), A closed-form solution for predicting the conductivity of porous media at low water content, *Soil Sci. Soc Am. J.*, 44, 892-898.
- Weissmann, G.S., E.M. LaBolle, and G.E. Fogg (2000), Modeling environmental tracer-based groundwater ages in heterogeneous aquifers. In, Bentley, L.R., Sykes, J.F., Brebbia, C.A., Gray, W.G., and Pinder, G.F. (eds.), *Computational Methods in Water Resources*, Volume 2:

Computational Methods, Surface Water Systems and Hydrology, Proceedings of the XIII International Conference on Computational Methods in Water Resources, Calgary, Alberta, Canada, June 25-29, 2000, A.A.Balkema, Rotterdam, p. 805-811.

Wilson, L.G. and K.J. Cook (1968), Field observations on changes in the subsurface water regime during influent seepage in the Santa Cruz River, *Water Resources Res.*, 4(6), 1219-1234.

FIGURE CAPTIONS

FIGURE 1. Location of collector wells within the SCWA facilities along the Russian River in Sonoma County, California and detail of the collector well.

FIGURE 2. Schematic of model domain.

FIGURE 3. Plan view of TOUGH2 grid.

FIGURE 4. Cross-sections of saturation (x-, y-, and z-plane) and pressure in Pascals (z-plane only) from Case 1c after 7 days of continuous pumping.

FIGURE 5. Cross-sections of saturation (x-, y-, and z-plane) and pressure in Pascals (z-plane only) from Case 1d after 7 days of continuous pumping.

FIGURE 6. Cross-sections of saturation (x-, y-, and z-plane) and pressure in Pascals (z-plane only) from Case 3d after 7 days of continuous pumping.

FIGURE 7. Velocity estimates near Collector Wells (CW) 1 and 2 from (a) seepage meters (Gorman, 2004) and (b) temperature profiles (Constantz et al., 2006).

FIGURE 8. Simulated pore velocities beneath the river at a location between the collector wells.

FIGURE 9. Normalized streambed fluxes as a function of time for Cases 1d and 4b, two of the cases where production at the well could not be sustained because the aquifer near the wells eventually desaturated.

FIGURE 10. Cumulative tracer breakthrough curves for (a) Case 1, (b) Case 2, and (c) Case 3.

TABLE 1. Summary of the simulation parameters

| Parameter | Aquifer (sand) | Streambed (silt) |
|---|---|--|
| Permeability (m ²) | 7.4 x 10 ⁻¹¹ and 2.4 x 10 ⁻¹⁰ | 7.4 x 10 ⁻¹³ to 2.4 x 10 ⁻¹⁰ |
| Porosity | 0.35 | 0.35 |
| Water density (kg/m ³) | 998.3 | 998.3 |
| Water viscosity (Pa s) | 1.00 × 10 ⁻³ | 1.00 × 10 ⁻³ |
| <i>Relative permeability</i> | | |
| <i>van Genuchten function (1980)</i> | | |
| Irreducible water saturation | 0.10 | 0.10 |
| Exponent | 0.457 | 0.270 |
| <i>Capillary pressure</i> | | |
| <i>van Genuchten function (1980)</i> | | |
| Irreducible water saturation | 0.05 | 0.05 |
| Exponent | 0.457 | 0.270 |
| Strength coefficient (m ⁻¹) | 5.9 | 0.64 |

TABLE 2. Summary of the permeabilities used in the simulations and peak travel times from the breakthrough curves.

| Case number | Aquifer permeability (m ²) | Streambed permeability (m ²) | k _{aquifer} /k _{streambed} | Maximum extent of unsaturated region in meters ⁴ (L x W x D) | Normalized volumetric streambed flux ¹ (m ³ /hr) | Normalized upstream boundary flux | Normalized downstream boundary flux |
|-----------------|--|--|--|---|--|-----------------------------------|-------------------------------------|
| 1a | 2.4 x 10 ⁻¹⁰ | 2.4 x 10 ⁻¹⁰ | 1 | saturated | 0.84 | 0.05 | 0.03 |
| 1b | 2.4 x 10 ⁻¹⁰ | 2.4 x 10 ⁻¹¹ | 10 | saturated | 0.97 | 0.04 | 0.03 |
| 1c | 2.4 x 10 ⁻¹⁰ | 2.4 x 10 ⁻¹² | 100 | 130 × 25 × 3 | 0.91 | 0.03 | 0.01 |
| 1d ³ | 2.4 x 10 ⁻¹⁰ | 7.4 x 10 ⁻¹³ | 324 | 470 × 60 × 13 | -- | -- | -- |
| 2a | 7.4 x 10 ⁻¹¹ | 7.4 x 10 ⁻¹¹ | 1 | saturated | 0.84 | 0.01 | 0.008 |
| 2b | 7.4 x 10 ⁻¹¹ | 7.4 x 10 ⁻¹² | 10 | 120 × 5 × 3 | 0.91 | 0.01 | 0.007 |
| 2c | 7.4 x 10 ⁻¹¹ | 5.4 x 10 ⁻¹² | 14 | 130 × 16 × 3 | 0.97 | 0.008 | 0.001 |
| 2d ³ | 7.4 x 10 ⁻¹¹ | 2.4 x 10 ⁻¹² | 31 | 160 × 40 × 13 | -- | -- | -- |
| 3a | 2.4 x 10 ⁻¹⁰ | 2.4 x 10 ⁻¹⁰ | 1 | saturated | 0.81 | 0.05 | 0.03 |
| | | 2.4 x 10 ⁻¹¹ | 10 | | | | |
| 3b | 2.4 x 10 ⁻¹⁰ | 2.4 x 10 ⁻¹⁰ | 1 | saturated | 0.78 | 0.05 | 0.03 |
| | | 2.4 x 10 ⁻¹² | 100 | | | | |
| 3c | 2.4 x 10 ⁻¹⁰ | 2.4 x 10 ⁻¹¹ | 10 | saturated | 0.88 | 0.04 | 0.03 |
| | | 2.4 x 10 ⁻¹² | 100 | | | | |
| 3d | 2.4 x 10 ⁻¹⁰ | 2.4 x 10 ⁻¹² | 100 | 150 x 60 x 3 | 0.81 | 0.03 | 0.001 |

| | | 2.4×10^{-13} | 1000 | | | | |
|-------------------|-----------------------|-----------------------|------|---------------|------|------|-------|
| 4a ² | 2.4×10^{-10} | 2.4×10^{-12} | 100 | 120 x 15 x 3 | 0.91 | 0.01 | 0.005 |
| 4b ^{2,3} | 2.4×10^{-10} | 7.4×10^{-13} | 324 | 400 x 60 x 13 | -- | -- | -- |

¹Normalized volumetric streambed flux calculated after 7 days of continuous pumping by dividing the total streambed flux by the pumping rate (3200 m³/hr).

²Cases 4a and 4b were conducted with a horizontal to vertical anisotropy ratio of 5. The remaining cases were conducted under isotropic conditions.

³Pumping rate of 3200 m³/hr was not sustained.

⁴Dimensions of the unsaturated region are the equilibrium size except for the cases where pumping was not sustained and the simulations stopped, occurring after 12.5 days in Case 1d, 2.5 days in Case 2d, and 7.8 days in Case 4b. The maximum extent of the unsaturated region when the simulations stopped is provided in the table.

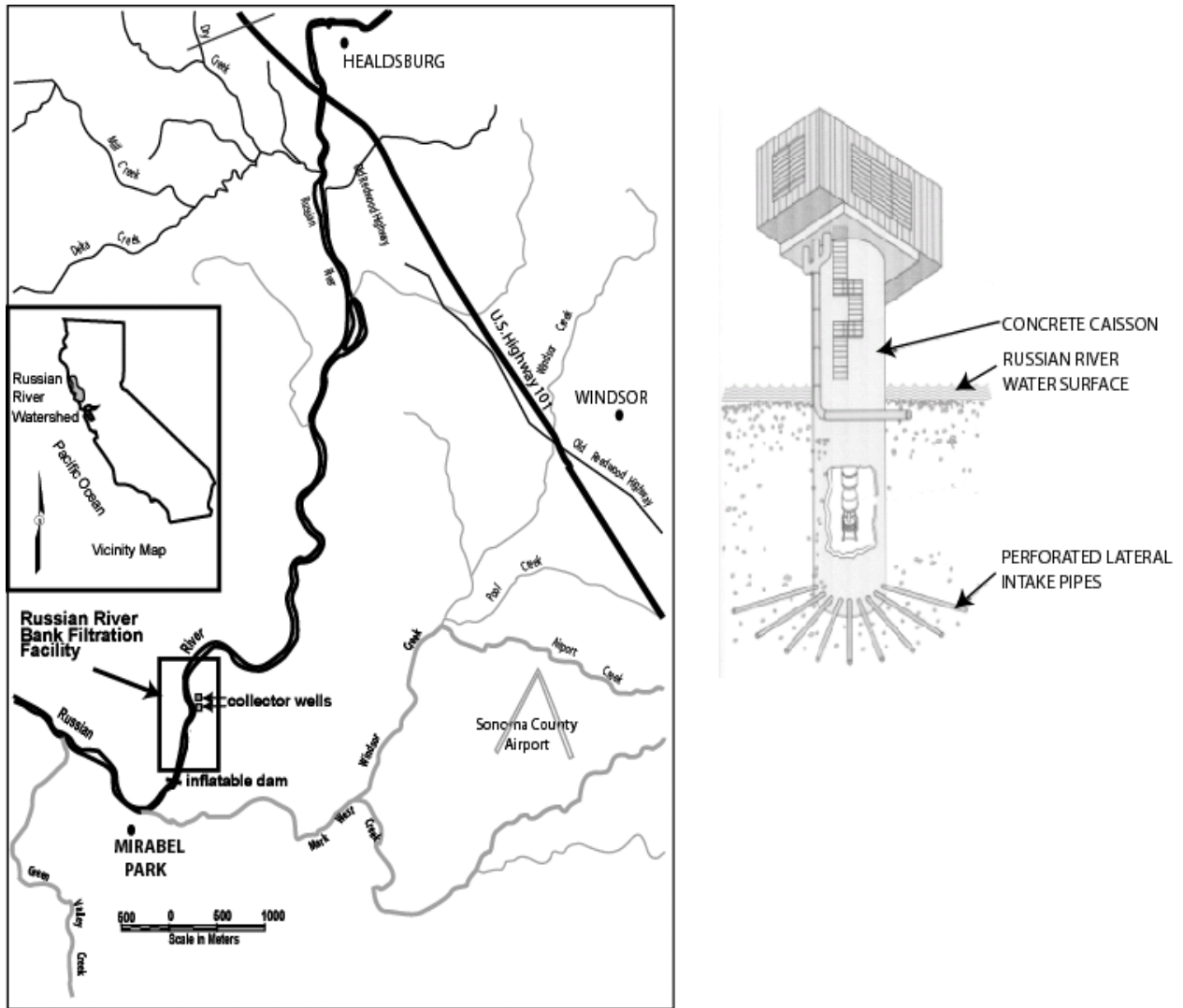


FIGURE 1. Location of collector wells within the SCWA facilities along the Russian River in Sonoma County, California and detail of the collector well.

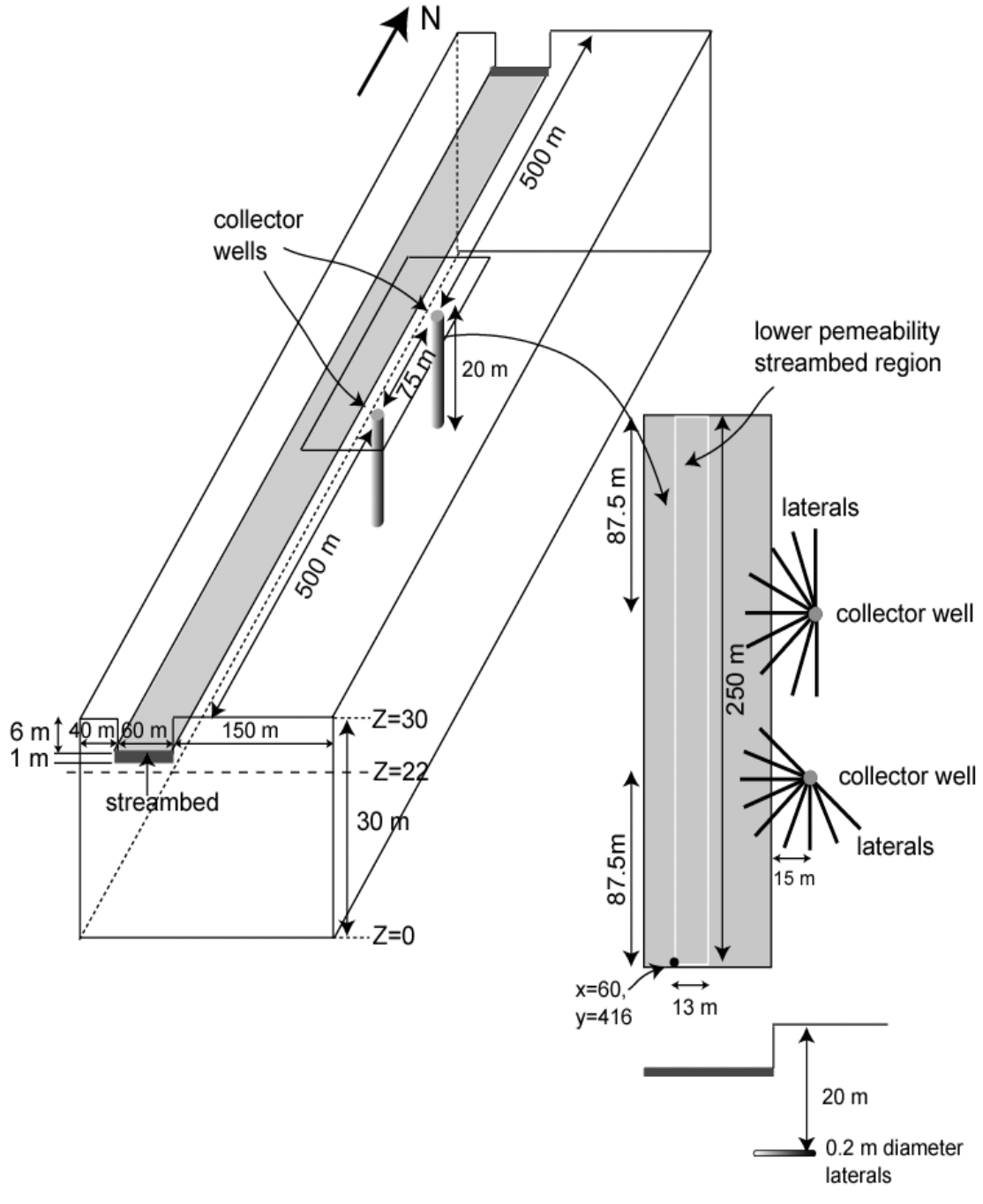


FIGURE 2. Schematic of model domain.

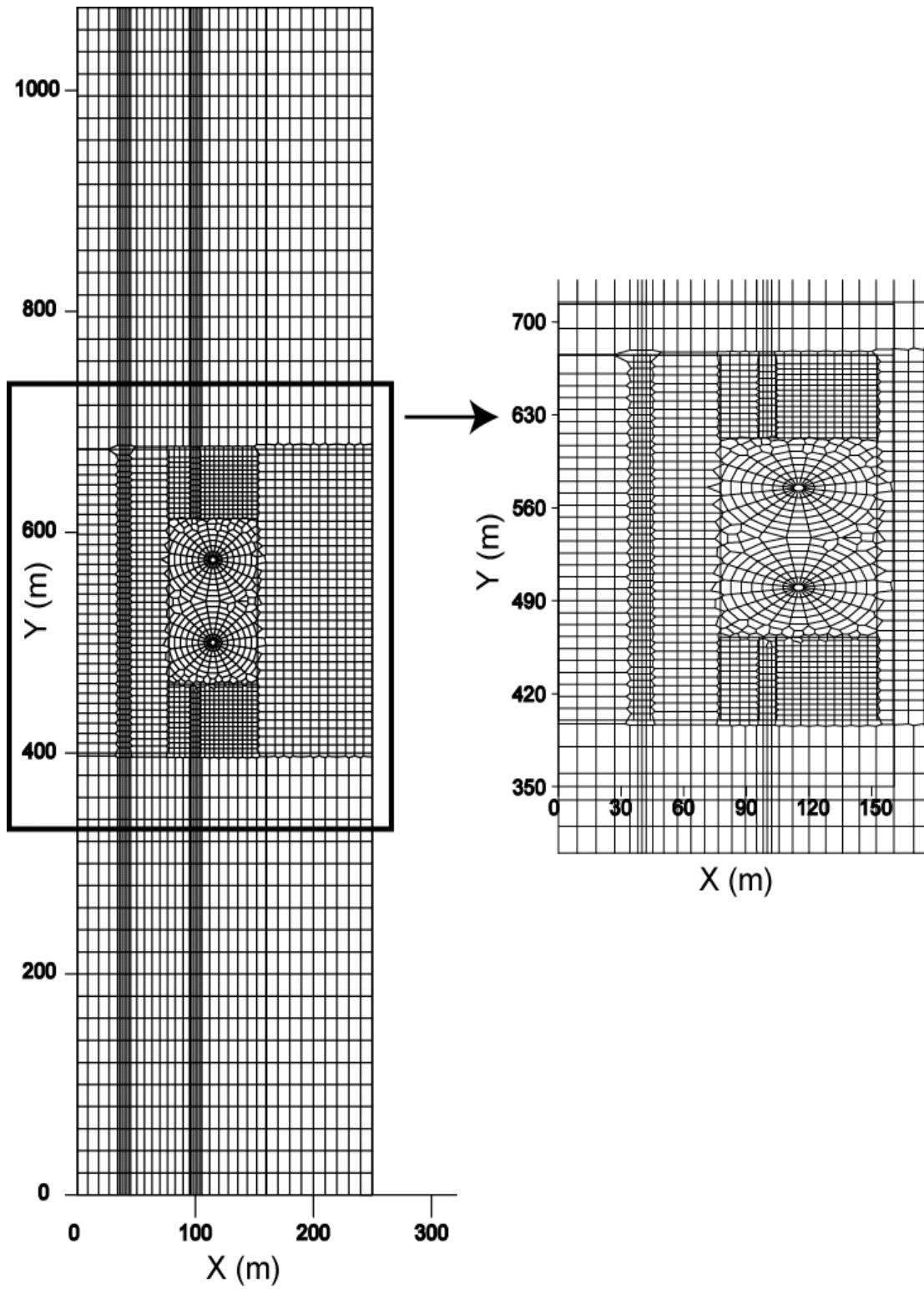


FIGURE 3. Plan view of TOUGH2 grid.

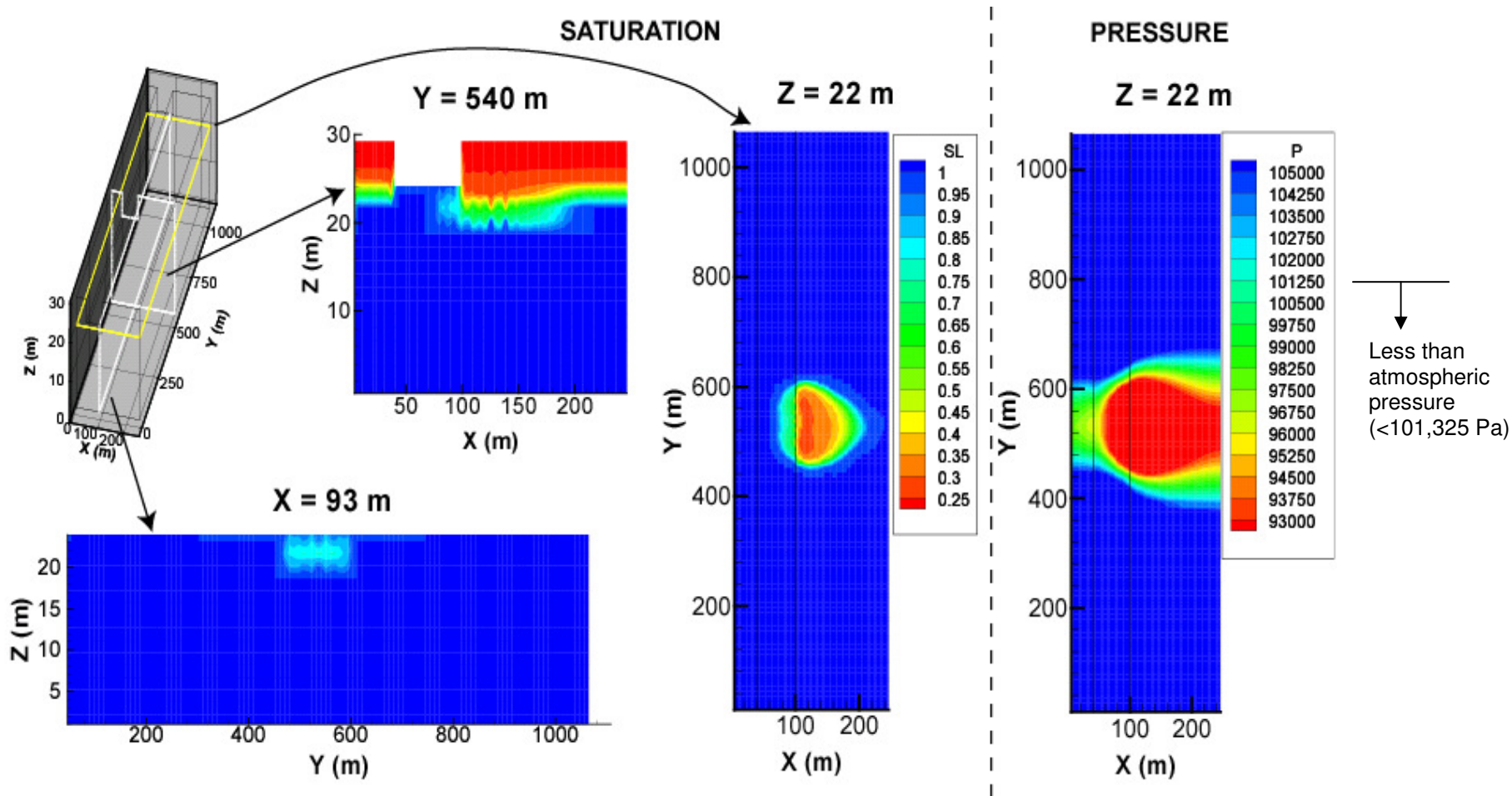


FIGURE 4. Cross-sections of saturation (x-, y-, and z-plane) and pressure in Pascals (z-plane only) from Case 1c after 7 days of continuous pumping.

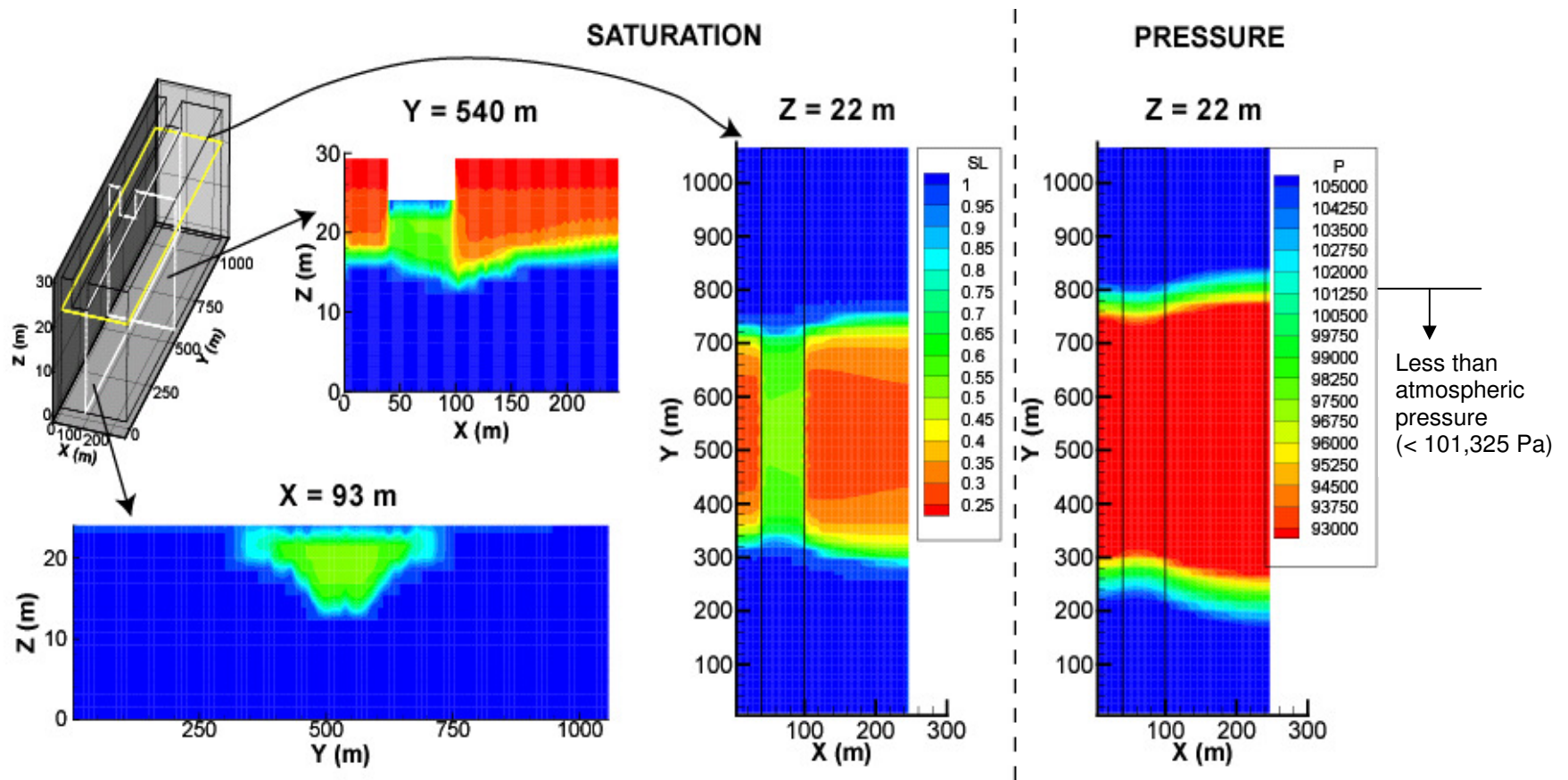


FIGURE 5. Cross-sections of saturation (x-, y-, and z-plane) and pressure in Pascals (z-plane only) from Case 1d after 7 days of continuous pumping.

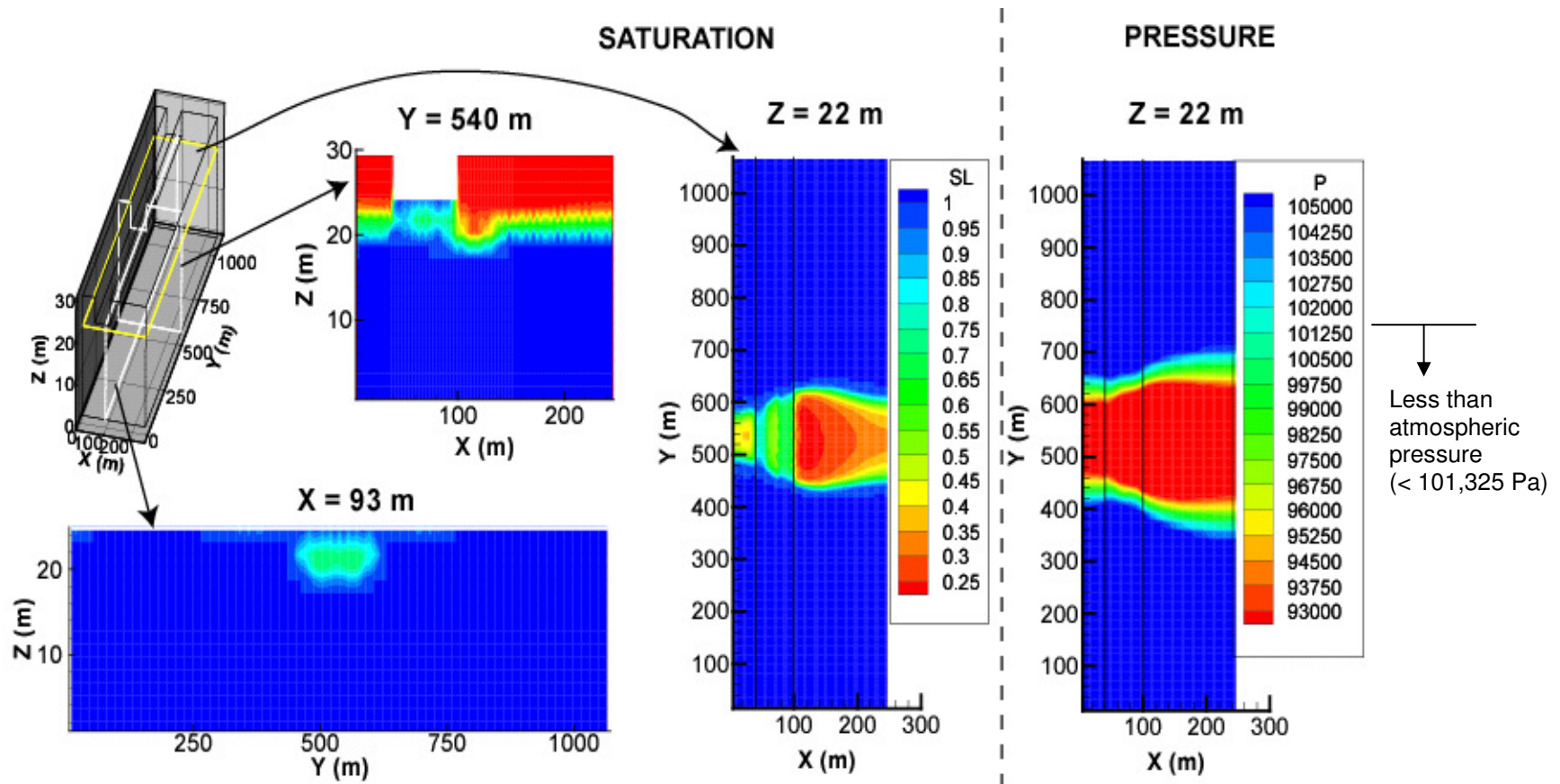
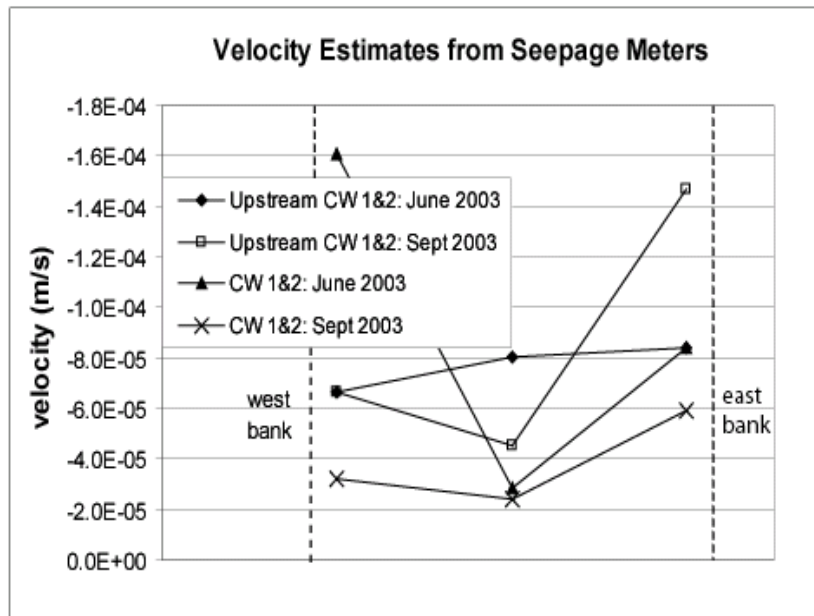
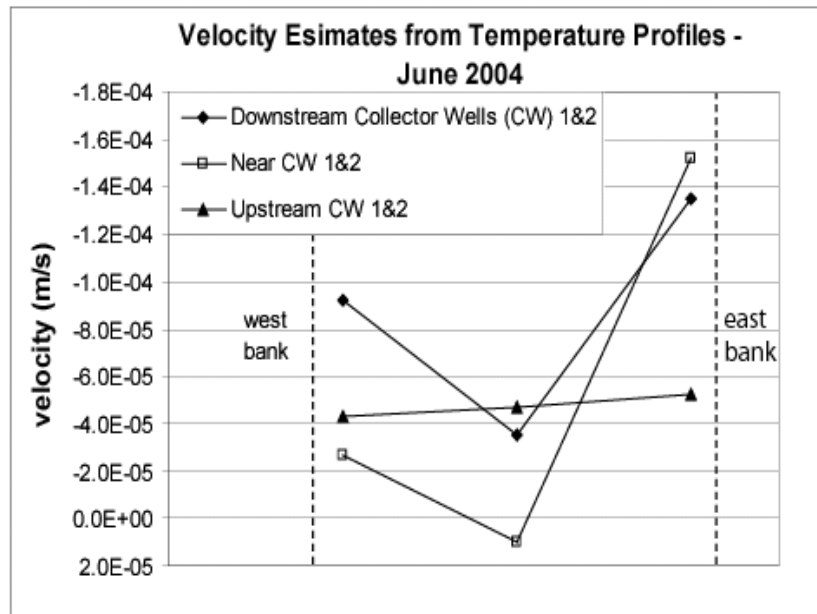


FIGURE 6. Cross-sections of saturation (x-, y-, and z-plane) and pressure in Pascals (z-plane only) from Case 3d after 7 days of continuous pumping.



(a)



(b)

FIGURE 7. Velocity estimates near Collector Wells (CW) 1 and 2 from (a) seepage meters (Gorman, 2004) and (b) temperature profiles (Constantz et al., 2006).

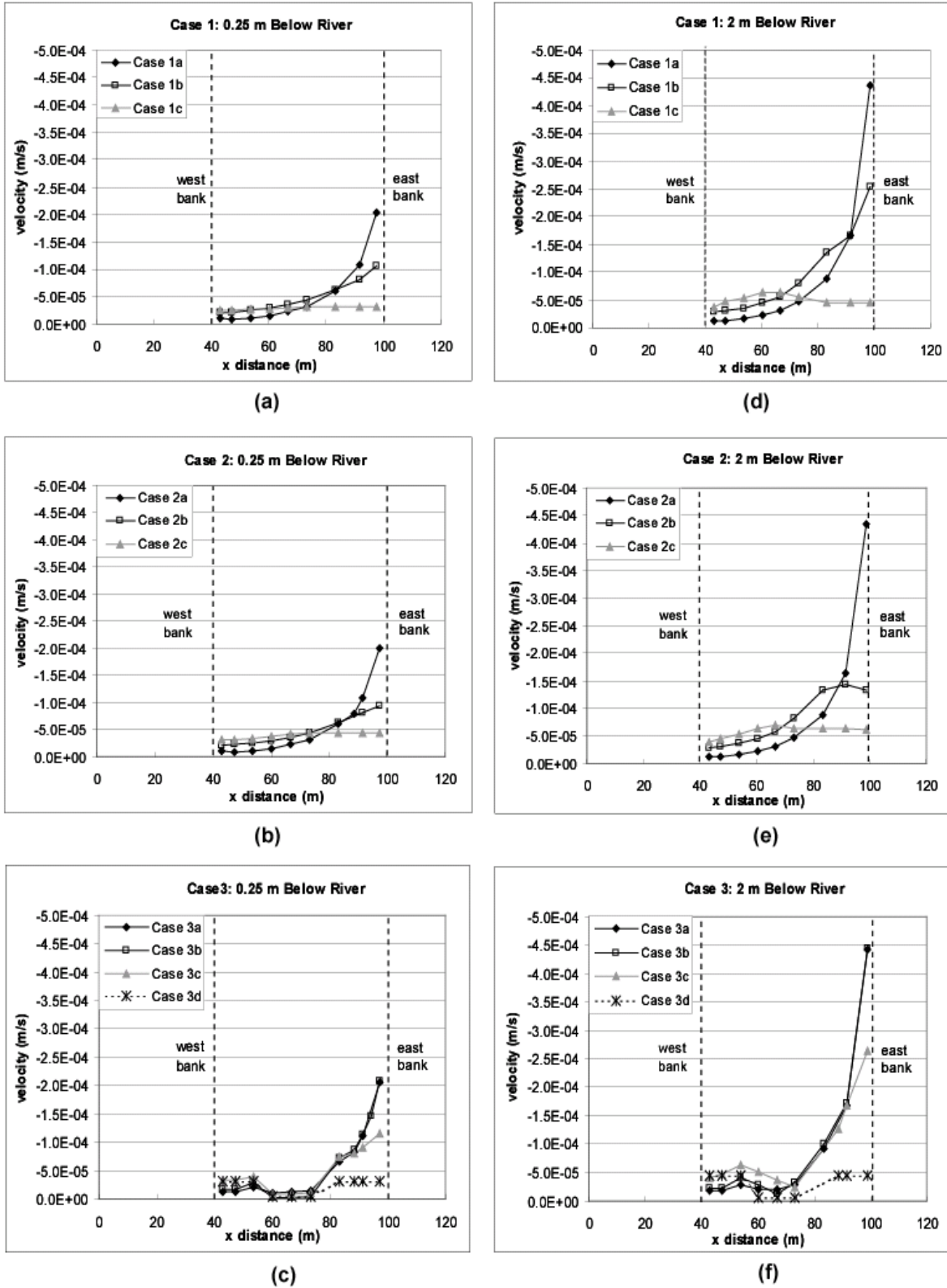


FIGURE 8. Simulated pore velocities beneath the river at a location between the collector wells.

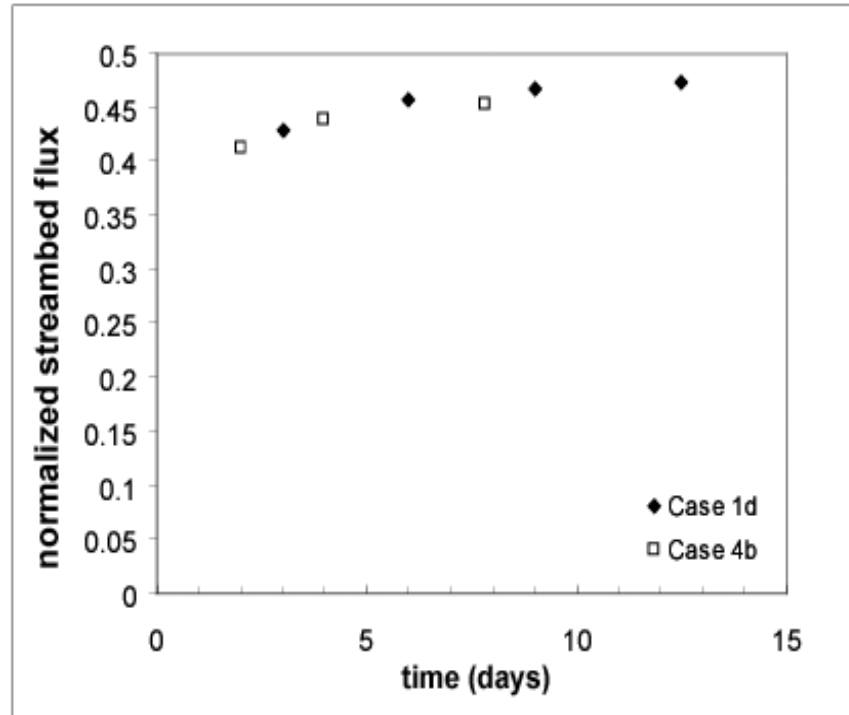


FIGURE 9. Normalized streambed fluxes as a function of time for Cases 1d and 4b, two of the cases where production at the well could not be sustained because the aquifer near the wells eventually desaturated.

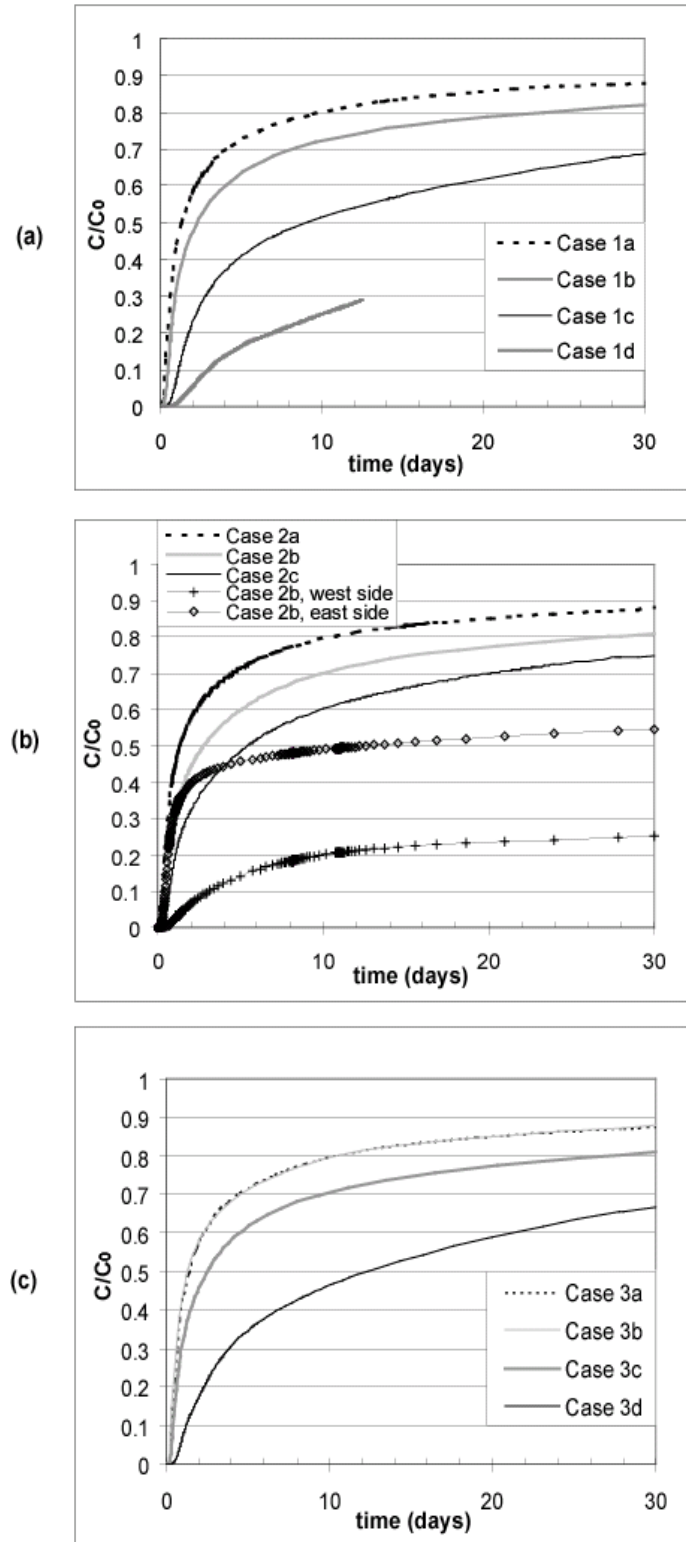


FIGURE 10. Cumulative tracer breakthrough curves for (a) Case 1, (b) Case 2, and (c) Case 3.